Nanoscale

COMMUNICATION

View Article Online
View Journal | View Issue

Cite this: *Nanoscale*, 2016, **8**, 12883

Received 16th May 2016,
Accepted 29th May 2016

DOI: 10.1039/c6nr03965k

www.rsc.org/nanoscale

Charge transfer at carbon nanotube–graphene van der Waals heterojunctions

Yuanda Liu,†[a] Fengqiu Wang,*†[a] Yujie Liu,[a] Xizhang Wang,[b] Yongbing Xu*[a] and Rong Zhang*[a]

Carbon nanotubes and graphene are two most widely investigated low-dimensional materials for photonic and optoelectronic devices. Combining these two materials into all-carbon hybrid nanostructures has shown enhanced properties in a range of devices, such as photodetectors and flexible electrodes. Interfacial charge transfer is the most fundamental physical process that directly impacts device design and performance, but remains a subject less well studied. Here, we complemented Raman spectroscopy with photocurrent probing, a robust way of illustrating the interfacial built-in fields, and unambiguously revealed both static and dynamic (photo-induced) charge transfer processes at the nanotube–graphene interfaces. Significantly, the effects of nanotube species, *i.e.* metallic as opposed to semiconducting, are for the first time compared. Of all the devices examined, the graphene sheet was found to be p-type doped with (6, 5) chirality-enriched semiconducting SWNTs (s-SWNTs), while n-type doped with highly pure (>99%) metallic SWNTs (m-SWNTs). Our results provide important design guidelines for all-carbon hybrid based devices.

Low-dimensional carbon allotropes, including one-dimensional carbon nanotubes (CNTs) and two-dimensional graphene, exhibit properties that are suitable for a wide range of optoelectronic applications such as photodetectors, light-emitting devices, and transparent electrodes.[1–5] These two materials share the same sp^2 hybridization of carbon atoms,[6] and can be merged into hybrid systems either covalently[7] or by van der Waals (vdW) interactions.[8–10] The hybrid system displays enhanced mechanical strength while retaining excellent optical and electrical properties, and is envisioned to offer optimized performance compared to the individual constituent materials.[11] For example, it has been recently demonstrated that high responsivities, and fast and broadband photo-detection can be achieved in a phototransistor based on a vdW bonded film consisting of single-wall carbon nanotubes (SWNTs) and graphene.[10] The construction of nanometer-scale one-dimensional vdW heterojunctions which can be harnessed in an optoelectronic device requires refined knowledge of the fundamental charge behavior at the nanotube–graphene interface, an important topic that remains less investigated.

To date, only a few previous reports have been dedicated to the study of electrostatic charge transfer at the nanotube–graphene heterojunctions,[12–14] typically *via* detecting characteristic peak shifts in Raman spectroscopy. Paulus *et al.* observed an electron transfer of 1.12×10^{13} cm^{-2} from an individual metallic SWNT to graphene, suggesting the presence of a relatively small potential offset between metallic SWNT and graphene.[12] Rao *et al.* synthesized SWNT bundles directly on graphene by chemical vapor deposition (CVD), but found that graphene donates electrons to the SWNT bundles.[13] It has been difficult to interpret and reconcile these seemingly contradictory results, and establish a generalized physical picture about the charge transfer scenario at the SWNT–graphene heterojunctions. In addition, both studies analysed only the Raman spectra, whereas the role photogenerated carriers may have played, an important aspect of the charge behavior at the interface, was not taken into consideration. Therefore, it is highly desirable to combine Raman spectroscopy with other examination tools to obtain deeper insights into the charge transfer dynamics at SWNT–graphene vdW heterojunctions.

Here, we address the limitations of previous studies by complementing Raman spectroscopy performed on atomically thin SWNT–graphene hybrid films, with associated photocurrent measurements. To this end, the photoresponse of a phototransistor based on the hybrid film is corroborated with the characteristic peak shifts as obtained in Raman spectroscopy, providing essential information about the built-in electric fields and the Fermi level information about the hybrid system. The robustness of this approach has for the first time enabled straightforward assignment of the electrostatic doping conditions at the SWNT–graphene interfaces. Our results

[a]*School of Electronic Science and Engineering and Collaborative Innovation Center of Advanced Microstructures, Nanjing University, Nanjing 210093, China. E-mail: fwang@nju.edu.cn, ybxu@nju.edu.cn, rzhang@nju.edu.cn*
[b]*School of Chemistry and Chemical Engineering, Nanjing University, Nanjing 210093, China*
† These authors contributed equally to this work.

unambiguously confirmed p-type (n-type) doping of graphene upon contact with semiconducting (metallic) SWNTs–graphene under dark conditions, and indicate that it will be possible to construct nanometer scale p–n junctions based on conduction-type modulation in a SWNT–graphene hybrid system.

The SWNT–graphene hybrid film is fabricated by transferring CVD-grown graphene onto the spin-coated SWNT layer, and the SWNT layers were spin-coated from the NMP (*N*-methyl-2-pyrrolidone) solution on the SiO_2 (285 nm)/Si substrate, as detailed in ref. 10. We characterized the carbon nanotubes on SiO_2/Si substrates with a FEI field emission SEM (Scanning Electron Microscopy), as shown in Fig. 1a. Most of the nanotubes appear straight and formed an atomically thin carbon nanotube network on the SiO_2/Si substrate. Meanwhile, due to the use of highly purified nanotubes, no metal catalyst particles are present, greatly mitigating the charge effects from extrinsic factors.

Raman spectroscopy is widely used for characterizing the electronic and structural properties of carbon materials and allows the determination of the doping level, intrinsic stress, and layer number of graphene. Raman spectra in this work were measured in the backscattering configuration. The scattered light was analyzed on a Horiba Jobin Yvon LabRAM HR 800 system using a 514 nm excitation laser operating at 1 mW, 100× objective lens with about ~1 μm beam spot diameter, and 1800 lines per mm grating with about 0.45 cm^{-1} spectral resolution. No polarization analyzer was used, so that light polarized both perpendicular and parallel to the scattering plane was collected. We first investigated the case where graphene comes in contact with (6, 5) chirality enriched (>93%) semiconducting s-SWNTs (Sigma-Aldrich). Fig. 1b shows the Raman spectrum of graphene, s-SWNT layer and s-SWNT/graphene hybrid, respectively. The black curve in Fig. 1b is a typical Raman spectrum of graphene with three featured peaks: D, G (~1589.7 cm^{-1}), and 2D (~2687.2 cm^{-1}) peaks. The D peak is due to the breathing modes of sp^2 rings and requires a defect for its activation.[15] The absence of the D peak indicates the defect-free nature of the graphene sample. The 2D peak can be fitted well by a symmetric and sharp Lorentzian peak with FWHM (Full Width at Half Maximum) ~26.2 cm^{-1}, a signature of single layer graphene. Also evident from the spectrum of graphene is an I_{2D}/I_G ratio of ~2.2 together with the area ratio A_{2D}/A_G ~6.6, indicative of monolayer graphene with reasonably good quality. The characteristic Raman modes of SWNTs[16] are the RBM (Radial Breathing Mode) (100–300 cm^{-1}), the G band (1500–1700 cm^{-1}), the D band (1300–1400 cm^{-1}) and the 2D band (2600–2700 cm^{-1}). Due to the curvature of the SWNTs, the G peak splits into two components G^- (at ~1542 cm^{-1}) and G^+ (at ~1586 cm^{-1}). For the SWNT/graphene hybrid material, the Raman features of graphene arising from the interfacial charge transfer under dark conditions include the shift of G and 2D band positions, a slight increase in the D peak, and a decrease of the I_{2D}/I_G ratio.

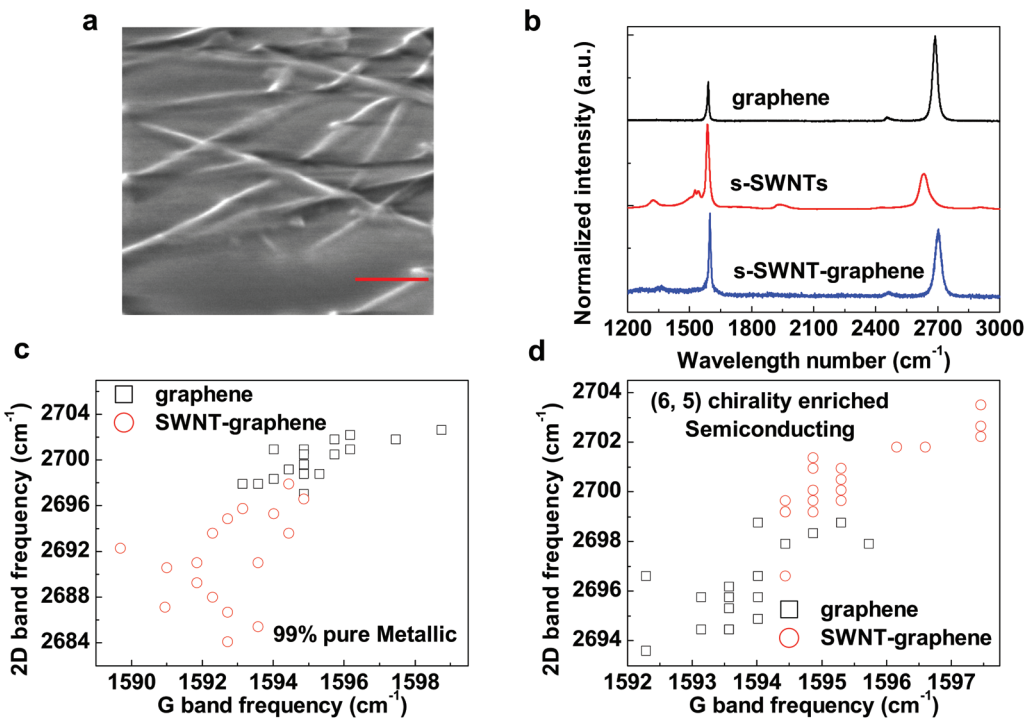

Fig. 1 (a) SEM micrograph of SWNTs on the SiO_2/Si substrate. Scale bar, 100 nm. (b) Raman spectroscopic characterization of graphene, SWNTs and SWNT–graphene hybrid, respectively. The laser power was kept at 1 mW to avoid the heating effect. (c) and (d) Peak positions of G and 2D Raman bands of graphene before and after coming into contact with 99% pure metallic and (6, 5) chirality enriched (>93%) semiconducting SWNTs, respectively.

A comparison of the G and 2D band positions of graphene before and after coming into contact with SWNTs is summarized, as shown in Fig. 1c and d. It should be noted that the data points shown correspond to Raman measurements on >15 different spots from each of the three regions: graphene only, SWNT only and SWNT–graphene hybrid regions (all three regions were on the same SiO_2/Si substrate and electrically isolated), in order to obtain generalizable doping information. Upon contact with 99% pure metallic SWNTs (m-SWNTs, Nanointegris), the G and 2D bands of graphene downshift by ~2.6 cm^{-1} and ~2 cm^{-1}, respectively. This indicates electron doping of the graphene sheet, or in other words, electrons transfer from metallic SWNTs to graphene, consistent with previous results.[12] For semiconducting SWNT–graphene scenario, it is found that both G and 2D peaks of graphene upshifts. Our finding of hole doping in the graphene sheet upon contact with s-SWNTs can be used to qualitatively support the observations made by Rao *et al.*,[13] in the case where semiconducting tubes constitute the main contribution for charge transfer.

To study the dynamic charge transfer, phototransistors using a SWNT–graphene hybrid as the channel are fabricated. The back-gated phototransistor devices are fabricated using standard photolithography, metal deposition by electron beam evaporation and lift-off. The electrical measurements were carried out in a closed cycle cryogenic probe station under vacuum (10^{-6} Torr) at room-temperature and the data were collected using a Keithley-4200 semiconductor parameter analyzer. Fig. 2a shows the transfer curves of the graphene and SWNT–graphene transistor measured in the absence of light. Compared with a pure graphene channel based transistor, the transfer curve of an s-SWNT–graphene transistor becomes asymmetric and the Dirac point (the charge neutrality point) shifts from about 3 V to a positive gate voltage of about 16 V, indicative of p-doping in the graphene sheet by semiconducting SWNTs. Fig. 2b illustrates the photoresponse of a semiconducting SWNT–graphene phototransistor under 650 nm laser light illumination. We observed that the illumination caused the Dirac point to shift leftward, and thus the source–drain current decreases for $V_G < V_D$(V_G, back-gate voltage. V_D, Dirac point voltage.) where the carrier transport is hole-dominated, but increases for $V_G > V_D$, where carrier transport is electron-dominated. Photocarrier generation at the graphene layer is negligible due to the ultrafast carrier recombination. Fig. 2c shows the photocurrent characteristics of a metallic SWNT–graphene phototransistor. Different from the s-SWNTs' case, it is observed that the transfer curve made a small but discernable shift towards a higher gate voltage with an increase in illumination above 650 nm, indicating that electrons transfer from the graphene sheet to metallic SWNTs, resulting in p-type photodoping of the graphene sheet. As junctions formed by metallic SWNTs and graphene are of the ohmic contact nature,[14] we attribute the photocarrier dynamics to the thermocouple effect, *i.e.* the hot electrons generated in the graphene sheet under light illumination are transferred to metallic SWNTs, resulting in the transfer curve shifting right.

Finally, we provide a qualitative, phenomenological and generalized physical picture underpinning previous[12–14] and present interfacial charge transfer observations in terms of the shifting of the Fermi level (E_F). When graphene is made to interface with metallic tubes, Fermi levels will be hybridized to an intermediate value. Due to the ohmic nature of the contact between the two materials, no built-in field is present at the interface. The dominating photocarrier

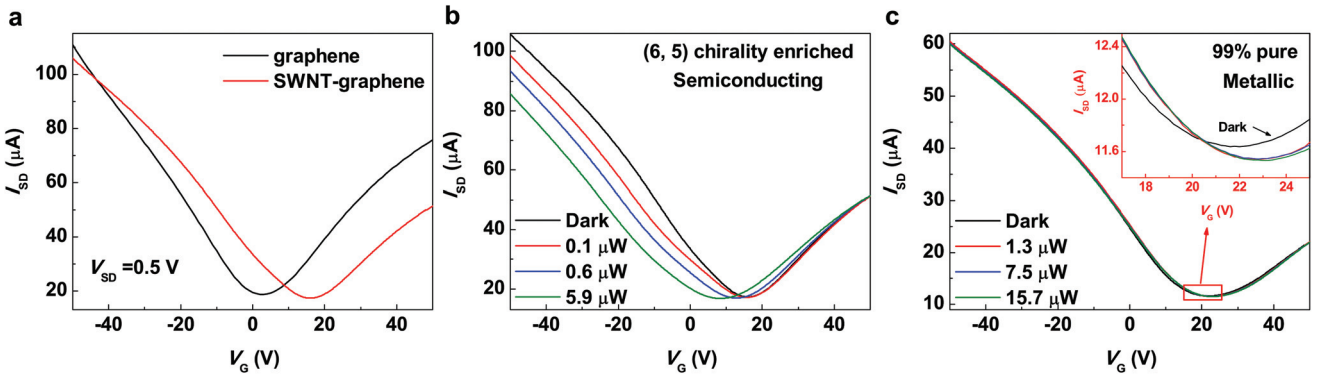

Fig. 2 (a) Transfer characteristics of graphene and s-SWNT–graphene phototransistor under dark conditions. It is shown that the Dirac point shifts to the right after s-SWNT functionalization. Source-drain voltage V_{SD} = 0.5 V. (b) Source–drain current characteristics of s-SWNT–graphene phototransistor as a function of back gate voltage under light excitation. Excitation wavelength is 650 nm. Increasing the illumination power leads to a photogating effect that shifts the Dirac point to the left, indicating that photogenerated electrons transfer from the s-SWNTs to graphene sheet, resulting in n-type photodoping of the graphene sheet. (c) Source–drain current characteristics of metallic SWNT–graphene phototransistor as a function of back gate voltage under light excitation. The inset shows the enlarged view of the section highlighted by the red rectangle. For metallic SWNTs, it is found that the transfer curve shifts toward positive V_G with the increase in the illumination power and the Dirac point shifts to the right. These observations indicate that electrons transfer from the graphene sheet to metallic SWNTs, resulting in p-type photodoping of the graphene sheet, which is opposite to the effect observed for semiconducting SWNT based hybrid devices. We attribute the observed phenomenon for metallic SWNTs' condition to the thermocouple effect. Hot electrons are generated in the graphene sheet under light illumination and transferred to metallic SWNTs, resulting in the transfer curve shifting right.

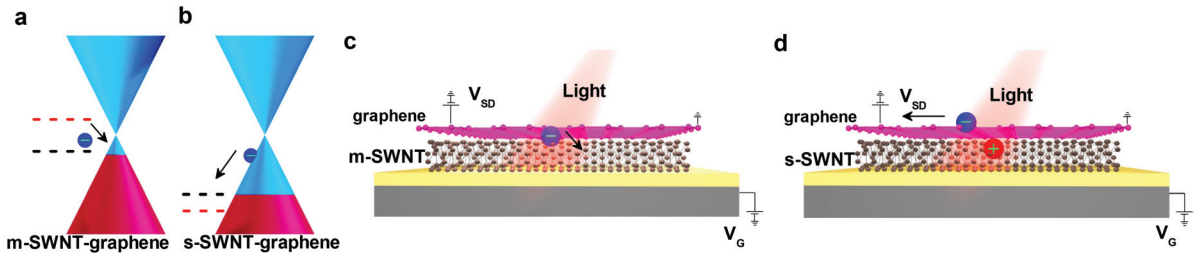

Fig. 3 (a) and (b) Schematic of Fermi level shifting in graphene before and after modification by metallic and semiconducting SWNTs, respectively (under dark conditions). Red and black dashed lines schematically denote the Fermi-levels in SWNTs under pre-equilibrium and equilibrium conditions, respectively. (c) and (d) Schematic diagram showing the photoexcited carrier transporting process at the interface between graphene and metallic or semiconducting SWNT, respectively. For metallic SWNTs, the photoresponse is governed by hot electrons originating in graphene. While for semiconducting SWNTs, a built-in electric field is established at the heterojunction. Photogenerated electrons in semiconducting SWNTs are transferred to graphene under the built-in field, leaving holes trapped in the SWNT.

dynamics is hot electrons in graphene transferring to metallic tubes. Our experimental findings support the view that CVD graphene tends to exhibit a lower Fermi level than metallic tubes, among various factors, CVD-grown graphene is known to be slightly p-doped due to the substrate oxide[17] (this unintentional p-doping is illustrated in Fig. 3a). Subsequently, when semiconducting SWNTs are considered (Fig. 3b), they also tend to lower the effective Fermi level of graphene (or m-SWNT–graphene hybrid), but with built-in electric fields established both at the s-SWNT–graphene interface and at the junctions where semiconducting and metallic nanotubes make contact. Upon photoexcitations of semiconducting SWNTs, photogenerated electron–hole pairs would separate under the built-in electric field, resulting in greatly enhanced photocurrent. The conceptual schematic diagrams were proposed to visualize the photoexcited carrier transferring process, as shown in Fig. 3c and d.

In conclusion, in contrast to the conventional method for studying the electrostatic doping scenario at the carbon nanotube–graphene interface, we for the first time complement Raman spectroscopy with photocurrent probing in SWNT–graphene based phototransistors. We uncover that charge transfer dynamics at SWNT–graphene heterojunctions are chirality-dependent and that a generalized physical picture can be utilized to interpret the interfacial electronic properties in a SWNT–graphene hybrid. Our results suggest that it will be possible to develop all-carbon hybrids with controllable electrical and optoelectrical behaviors by engineering nanoscale architectures with customized SWNT chiralities, and provide important design guidelines for novel devices based on this emerging low-dimensional hybrid material.

This work was supported in part by the National Key Basic Research Program of China 2014CB921101, 2011CB301900, 2013CBA01604; the National Natural Science Foundation of China 61378025, 61450110087, 61427812, 61274102; Jiangsu Province Shuangchuang Team Program. Y. D. L. acknowledges funding of National Natural Science Foundation of China 61504056, International Postdoctoral Exchange Fellowship Program 20150023, the China Postdoctoral Science Foundation 2014M551558 and Jiangsu Planned Projects for Postdoctoral Research Funds 1402028B.

References

1 A. K. Geim and K. S. Novoselov, *Nat. Mater.*, 2007, **6**(3), 183.
2 P. Avouris, M. Freitag and V. Perebeinos, *Nat. Photonics*, 2008, **2**(6), 341.
3 P. Avouris, Z. Chen and V. Perebeinos, *Nat. Nanotechnol.*, 2007, **2**(10), 605.
4 J. Misewich, R. Martel, P. Avouris, J. Tsang, S. Heinze and J. Tersoff, *Science*, 2003, **300**(5620), 783.
5 M. Freitag, J. Chen, J. Tersoff, J. C. Tsang, Q. Fu, J. Liu and P. Avouris, *Phys. Rev. Lett.*, 2004, **93**(7), 076803.
6 K. S. Novoselov, A. K. Geim, S. V. Morozov, D. Jiang, Y. Zhang, S. V. Dubonos, I. V. Grigorieva and A. A. Firsov, *Science*, 2004, **306**(5696), 666.
7 Z. Yan, Z. Peng, G. Casillas, J. Lin, C. Xiang, H. Zhou, Y. Yang, G. Ruan, A. R. O. Raji and E. L. Samuel, *ACS Nano*, 2014, **8**(5), 5061.
8 X. Lin, P. Liu, Y. Wei, Q. Li, J. Wang, Y. Wu, C. Feng, L. Zhang, S. Fan and K. Jiang, *Nat. Commun.*, 2013, **4**, 2920.
9 I. N. Kholmanov, C. W. Magnuson, R. Piner, J. Y. Kim, A. E. Aliev, C. Tan, T. Y. Kim, A. A. Zakhidov, G. Sberveglieri and R. H. Baughman, *Adv. Mater.*, 2015, **27**(19), 3053.
10 Y. Liu, F. Wang, X. Wang, X. Wang, E. Flahaut, X. Liu, Y. Li, X. Wang, Y. Xu, Y. Shi and R. Zhang, *Nat. Commun.*, 2015, **6**, 8589.
11 R. Lv, E. Cruz-Silva and M. Terrones, *ACS Nano*, 2014, **8**(5), 4061.
12 G. L. C. Paulus, Q. H. Wang, Z. W. Ulissi, T. P. McNicholas, A. Vijayaraghavan, C. J. Shih, Z. Jin and M. S. Strano, *Small*, 2013, **9**(11), 1954.
13 R. Rao, N. Pierce and A. Dasgupta, *Appl. Phys. Lett.*, 2014, **105**(7), 073115.
14 T. Pei, H. Xu, Z. Zhang, Z. Wang, Y. Liu, Y. Li, S. Wang and L. Peng, *Appl. Phys. Lett.*, 2011, **99**(11), 113102.
15 T. M. G. Mohiuddin, A. Lombardo, R. R. Nair, A. Bonetti, G. Savini, R. Jalil, N. Bonini, D. M. Basko, C. Galiotis and N. Marzari, *Phys. Rev. B: Condens. Matter*, 2009, **79**(20), 205433.
16 A. Kukovecz, C. Kramberger, V. Georgakilas, M. Prato and H. Kuzmany, *Eur. Phys. J. B*, 2002, **28**(2), 223.
17 W. J. Yu, Y. Liu, H. Zhou, A. Yin, Z. Li, Y. Huang and X. Duan, *Nat. Nanotechnol.*, 2013, **8**, 952.